RSC Advances

ROYAL SOCIETY OF CHEMISTRY

www.rsc.org/advances

Journal Name

ARTICLE

The importance of raw graphite size to the capacitive properties of graphene oxides

Received 00th January 20xx,
Accepted 00th January 20xx

DOI: 10.1039/x0xx00000x

www.rsc.org/

Haoran Yu[a], Keyu Xie[a,*], Jingzhi Hu[a], Chao Shen[a], Jian-gan Wang[a], Bingqing Wei[a,b]*

Carbon-based materials have been widely used in energy storage and conversion devices. Among them, graphene oxide (GO) holds much promise for supercapacitor applications due to its high-capacitance, low-cost, etc. Nevertheless, intrinsic characteristics related to capacitive properties of GO are far from being fully understood. Little attention has been paid to the size effect of raw graphite on electrochemical characteristics of GO. In order to investigate the relationship between raw graphite size and capacitive properties of GO, the electrochemical performances of GO, prepared from raw graphite with three different sizes using modified Hummer's method, were compared. Experimental results indicated that the capacitance of the GO electrode enhanced with the increasing size of the raw graphite. The GO electrode prepared with the largest size achieved a specific capacitance as high as 94.4 F g^{-1} at 0.1 A g^{-1} due to medium-sized specific surface area and smaller charge transfer resistance. It is concluded that more attention should be paid on the prevention of agglomeration or even restacking of the graphene-based material, after the heat drying of graphene-based solutions because of residual intercalated water molecules, which contribute to strong hydrogen bonding interactions between layers.

Introduction

With the development of society and economy, energy crisis and environmental pollution are becoming the most important issues[1-3]. There is a high demand for environmental friendly and novel renewable energy power sources. With fast and safely charged/discharged capability, long-term cycle stability and excellent reversibility, supercapacitors, also called electrochemical capacitors or ultracapacitors, are becoming attractive substitute sources[4-6].

In a common supercapacitor, carbon materials play a principal and irreplaceable role in its energy-store performance[7-9]. Up to now, there is a wide variety of carbon-base materials served as electrodes for supercapacitors, including activated carbons, carbon gels, carbon fibers, carbon nanotubes, graphene, and graphene oxide (GO)[10]. Among them, graphene has high electrical conductivity and a large theoretical surface area of 2670 m^2 g^{-1}, for which it's an ideal electrode material of supercapacitors. However, there are more or less short-comings in the synthesis of high quality graphene: mechanical exfoliation of graphite flakes is a serendipitous method, and this technique only contributes to uneven films and is not suitable for large-scale production; epitaxial growth is a high-temperature process beyond control of morphology and adsorption energy; a reduction of GO is a promising approach but reduction to graphene is only partial with a fragile stability of the colloidal dispersion[11-13]. Therefore, it still needs to compete with activated carbons in terms of cost/performance to be utilized in actual production. Nonetheless, the intermediate GO bears interesting potentials as a supercapacitor electrode material owing to its low cost and high capacitance. During the formation of GO, it disrupts the conjugated structure and localizes π-electrons by embedding covalent functional groups. Afterwards, covalent functional groups enhance the total capacitance through pseudo-capacitance. Also, they are functional sites and offer more opportunities for a secondary modification, such as doped with nitrogen or phosphorus[14]. Taking its lower cost and high capacitance into account, GO may be a better choice than graphene as an electrode material for supercapacitors[15]. The capacitance up to 159 F g^{-1} in H_2SO_4 and 82 F g^{-1} in $(C_2H_5)_4NBF_4$/acetonitrile were reported for GO[10], and they show a much higher volumetric capacitance than the majority of carbons, which is a key factor for the development of energy storage devices. A higher capacitance up to 189 F g^{-1} was obtained with GO electrodes in a symmetrical two-electrode cell[15]. However, little attention has been focused on size effect of raw graphite on the electrochemical characteristics of GO for supercapacitors. It would be valuable to study the relationship between raw material size and the electrochemical performances of GO.

Herein, this paper mainly addresses the comparison on electrochemical performances of GO prepared by a modified Hummers method from three different raw graphite sizes. It was found that the capacitance of the GO electrode is enhanced with increasing size of the raw graphite. In addition, how to prevent GO

[a] State Key Laboratory of Solidification Processing and Center for Nano Energy Materials, Northwest Polytechnical University, Xi'an 710072, China.
[b] Department of Mechanical Engineering, University of Delaware, Newark, DE19716.Email: weib@udel.edu; Phone: 1-302-831-6438; Fax: 1-302-831-3619

*Corresponding author.
E-mail address: kyxie@nwpu.edu.cn (K.Y. Xie); weib@udel.edu (B.Q. Wei)
Electronic Supplementary Information (ESI) available: [details of any supplementary information available should be included here]. See DOI: 10.1039/x0xx00000x

from agglomeration or even restacking is also discussed. Our work will provide a practical guidance to the synthesis of GO-based electrode materials for supercapacitors.

Experimental

Synthesis of GO

GO was prepared using a well-known modified Hummer's method, which has been described in detail elsewhere[16, 17].The raw materials were natural graphite particles with sizes of 80~120 mesh, 750~850 mesh, and 2000 mesh (Aladdin), and the corresponding samples were designated as GO (100 mesh), GO (800 mesh), and GO (2000 mesh), respectively. Briefly, these raw graphite particles (0.5 g) were preoxidized with sulfuric acid (25 ml) for 30 min at room temperature. And then, sodium nitrate (0.5 g) and potassium permanganate (3 g) were slowly dispersed into the mixture, immediately transferred into an ice bath with temperature below 20 °C for 2 h. Next, this mixture was stirred when temperature is increased to 35 °C. After oxidizing for 3 h, the mixture obtained was diluted with 140 ml deionized water and stirred for another 2 h when heated to a temperature of 95 °C. And then, hydrogen peroxide was poured into the mixture until the color changed from nigger-brown to light yellow with no air bubbles generated. Afterwards, the solution obtained was washed with deionized water till the pH value became 6~7 to obtain GO. The GO suspension was sonicated for 30 min with a power about 200 W. After a short rest for about 10 min, the suspension was ultrasonicated for 10 min (UP400S, 0.4 cycle, 80% intensity). The procedure above was repeated for three times and the GO dispersion was obtained after centrifugation. Finally, the GO dispersion was dried at 80 °C in an air dry oven for about 24 h to get GO.

Characterization techniques

The GO morphology was characterized using scanning electron microscope (SEM, JSM6700E) and transmission electron microscope (TEM, JEOL JEM-3010F). Raman spectra were obtained by HORIBA JOBIN YVON HR 800 and Renishan inVia instrument. X-ray photoelectron spectroscopy (XPS) was performed on an ESCALAB250xi XPS system. XRD data were measured in an X-ray diffractometer (Rigaku Tokyo, Japan) D/max-2400. The Nitrogen adsorption-desorption isotherms of the samples were determined by Surface Area and Porosity Analyzer (ASAP 2020 HD88). The square resistances were tested by four-point probe meter (SZT-2A).

Electrochemical measurements

The electrochemical performance was tested on workstation (Solartron analytical 1400+1470E) using a three-electrode system at room temperature. Consequently, nickel foam (15 mm × 15 mm) dipped into the active material slurry was selected as the working electrode. The active material (about 4 mg per electrode after drying) contained GO, carbon black and Polyvinylidene Fluoride (PVDF) binder with a mass ratio of 7:2:1 dissolved in N-Methyl pyrrolidone (NMP). The electrode was dried at 60 °C in a vacuum oven for 24 h. At last, the nickel foam coated with the active materials as the working electrode, a platinum foil as the counter electrode, a saturated calomel electrode as the reference electrode, and 6 M potassium hydroxide solution as electrolyte were used. Cyclic voltammetry (CV) was performed with a potential window from -0.8 V to 0 V at different scan rates (5, 10, 20, 30, and 50 mV s^{-1}). Galvanic cycle (GC) was carried out with a voltage from -0.7 V to 0 V at various current densities (0.1, 0.2, 0.5, 1, and 2 A g^{-1}). In addition, the cyclic stability of the GO electrodes at a current density of 1 A g^{-1} for 1500 cycles was measured by GC. Electrochemical Impedance Spectroscopy (EIS) measurement was performed over a frequency range from 0.01 Hz to 10 kHz.

Results and discussion

Morphological and structural characterizations

The shape, size and intrinsic structure of raw graphite powers are characterized using SEM, whose images of graphite powers with 2000 mesh, 850~750 mesh and 120~80 mesh are presented in Fig. 1(a-c). In Fig. 1(a), the particles have a wide particle distribution but basically particle size is less than 20 μm. As indicated in Fig. 1(b), the particle size is about 20 to 40 μm. Fig. 1(c) shows the relatively integrated slice of graphite with a size of more than 100 μm. Fig. 1(d) gives a TEM image of GO (2000 mesh) prepared by the modified Hummer's method. It demonstrates clearly that the prepared GO shows silk veil-waves morphology with thin nanosheets.

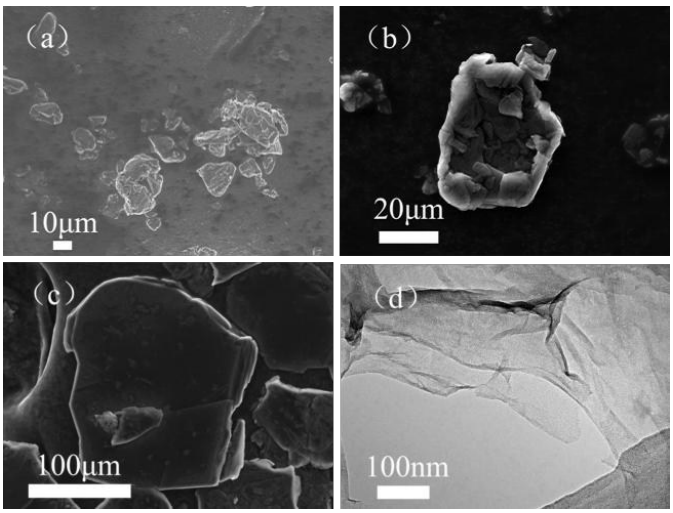

Fig. 1. SEM images of the raw graphite (a) graphite 2000 mesh, (b) graphite 850~750 mesh and (c) graphite 120~80 mesh, (d) TEM image of GO (2000 mesh).

It is well known that the G band of a Raman spectrum is a typical representation of the E_{2g} vibrational modes of the aromatic domains, whereas the D band is generated from the breathing modes of the graphitic domains[18-21]. As shown in Fig. 2, obvious D and G bands are located at 1354 cm^{-1} and 1591 cm^{-1}, respectively, of the latter shifts a bit from graphite Raman spectrum peak (1580 cm^{-1}) after chemical oxidation. In addition, the intensity ratio of D band to G band (I_D/I_G) is used to estimate the disorder degree of graphene[18]. Compared to raw graphite, the I_D/I_G of all the GOs obtained from

different graphite sizes were increased dramatically, indicating high disorders of the GOs, arising from the addition of oxygen-containing functional groups[22]. However, the sizes of raw graphite have almost no effect on Raman spectrum, showing the three samples have similar graphitic degree.

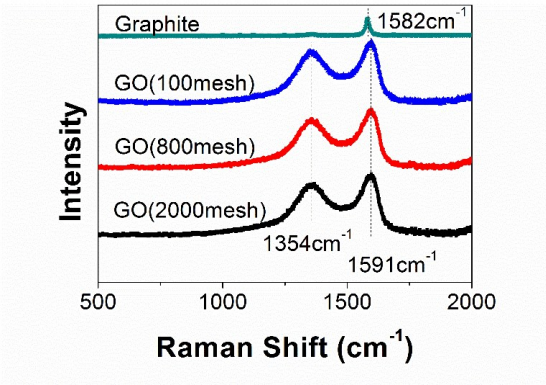

Fig. 2. Raman spectra of GO (2000 mesh), GO (800 mesh), GO (100 mesh) and graphite.

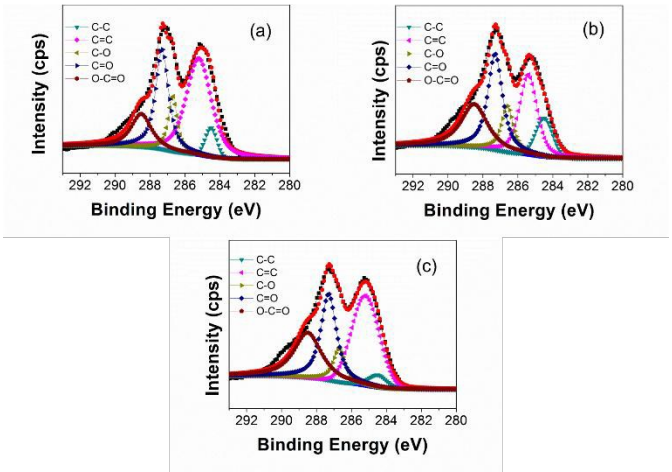

Fig. 3. XPS spectra of C1s in (a) GO (2000 mesh), (b) GO (800 mesh), (c) GO (100 mesh).

XPS characterizations are further employed to analyze the elemental compositions and the configurations of oxygen-containing functional groups in GO. The binding energy of C-C is located at around 284.5 eV, and therefore the peaks of oxygen-containing functional groups added to graphite have a shift with respect to C-C bind. In Fig. 3(a), the C1s spectrum of the GO (2000 mesh) can be fitted into five peaks centered at 284.5, 285.2, 286.7, 287.2, and 288.6 eV, which could be assigned to the non-oxygenated ring C atoms, or says sp^3C (C-C) and sp^2C (C=C), the C atoms in the epoxy/ether groups (C-O), the carbonyl C structure (C=O), and the carboxyl C structure (O-C=O), respectively [23]. It can be clearly seen that the XPS spectra of GO (800 mesh) (Fig. 3(b)) and GO (100 mesh) (Fig. 3(c)) are similar to that of GO (2000 mesh). Meanwhile, the molar ratios of C/O of GO (2000 mesh), GO (800 mesh), and GO (100 mesh) are obtained to be 2.2, 2.1, and 2.2, respectively, indicating that the oxidation of three different raw materials are at almost the same level.

Fig. 4 shows the XRD patterns of raw graphite, GO (2000 mesh), GO (800 mesh), and GO (100 mesh). The XRD pattern of raw graphite appears a basal reflection (002) with the sharp peak at 26.5 °, and as for GO, a broad peak corresponding to diffraction (001) is found to be at 2θ=11.3°, 11.2° and 10.9°, respectively. According to the following Bragg equation:

$$2d\sin\theta = n\lambda \quad (1)$$

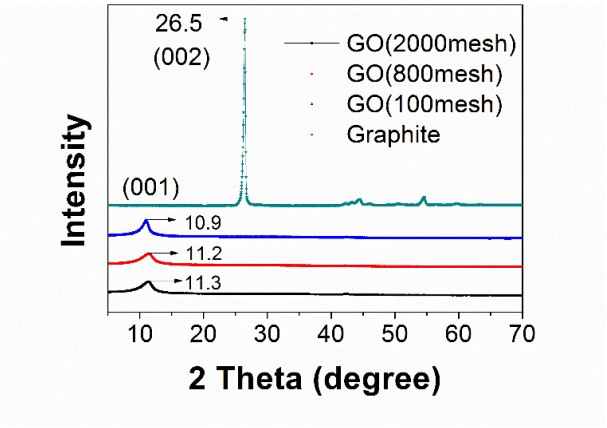

Fig. 4. XRD patterns of GO (2000 mesh), GO (800 mesh), GO (100 mesh) and graphite.

where d is the interlayer spacing of GO, θ is diffraction angle, n is the number of interlayers, and λ is the X-ray wavelength of Cu target, the interlayer spacing of GO (2000 mesh), GO (800 mesh) and GO (100 mesh) can be easily calculated to be 0.782 nm, 0.789 nm and 0.811 nm, respectively. According to the results of Raman and XPS, the oxidation degree of the three samples is similar. However, it is interesting to notice that the interlayer spacing increases with the increase of particle sizes. This phenomenon appeared maybe caused by the hydrogen bonding interactions: the interesting thing is that the "intercalated" water molecules remain stuck in the GO particles via hydrogen bonding interactions which facilitates interactions between GO sheets, resulting in spontaneously agglomerate and even restack to form graphite oxide after the GO solution is dried[8, 24-26]. Moreover, different sized particles can cause different degrees of oxidation (the carbon atoms between layers not from edges), which had influence on interlayer spacing between GO layers.

The hypothesis mentioned above is exactly substantiated by previous work[23, 27]. The formation of pristine GO covers the diffusion of the oxidizing agent into the graphite interlayer galleries and followed by a chemical reaction. Above all, this is the rate-determining step, which is diffusive-controlled where the oxidant replaces the acid intercalant[27]. Consequently, graphite with small size is oxidized significantly faster than a large one corresponding to more oxygen-containing functional groups between the layers under the same oxidation degree, which contributes to strong hydrogen bonding interactions. Hence, hydrogen bonding interactions lead to the different interlayer spacing of three samples, after heat drying of GO solution, which is well coincided with XRD patterns. It is apparent that, in the preparation with GO, it would spontaneously agglomerate if there is no protective measures by heat drying GO solution.

Nitrogen adsorption-desorption isotherms at 77 K and the pore size distributions of the three samples are shown in Fig. 5. It is

observed that all three samples belong to type-I species according IUPAC classification[28-30]. The type-I isotherm evidently levels off below the relative pressure of 0.1 indicating that the GO samples are exclusively microporous. Moreover, the pore size distribution curves based on nonlinear density functional theory (NLDFT) confirm that the majority of these pores of three GO samples were found less than 2 nm in diameter. As shown in Fig.5, GO (2000 mesh), GO (800 mesh) and GO (100 mesh) have an undeveloped porosity with a specific surface area of 32, 89 and 62 $m^2 g^{-1}$, respectively, which are contributed by the defects and structure of GO. The data obtained here are a little lower than previous results[15]. This result may be attributed to the agglomeration or even restacking of GO, destroying the pore structure and thus reducing the specific surface area. As for smaller particles, GO (2000 mesh) originally tend to own a larger surface area, however, they contain more oxygen functional groups so that the stronger hydrogen bonding interactions would lead to greater damage of structure. This could be the reason that the specific surface area of GO (2000 mesh) is lower than that of GO (800 mesh). Evidently, GO suffers from severe restacking between individual sheets and thus loses its material identity and advantages. Therefore, the most important and challenging hurdle to achieve a high capacitance is to hinder the restacking of the GO sheets. One of the problem solving approaches is the use of nonpolar aprotic "solvent", which doesn't have any interaction with those oxygen groups of GO, thereby leading to the formation of crumpled non-stack GO. For example, hydrophobic hexane as an anti-solvent was introduced to fabricate highly crumpled non-stacked GO nanosheets. By using hexane, it could be easily seen that the diffraction peak of GO was shifted from 11.38° to 10.36°[24]. Another solution to eliminate the hydrogen bonding is by a condensation reaction of the hydroxyl end groups of polymer monomers with the hydroxyl or carboxylic acid groups on the GO sheets. For instance, GO was functionalized in the solution state with melamine resin monomers and successfully prevented the hydrogen bonding interactions[26]. In fact, rapid freeze-drying may be useful to remove water molecules. Because the fluffy porous structure could be maintained by freezing in less than 5 seconds. For example the specific area of GO (100 mesh) can be improved to 158 $m^2 g^{-1}$ using rapid freeze-drying. (Supporting Information Fig. S1)

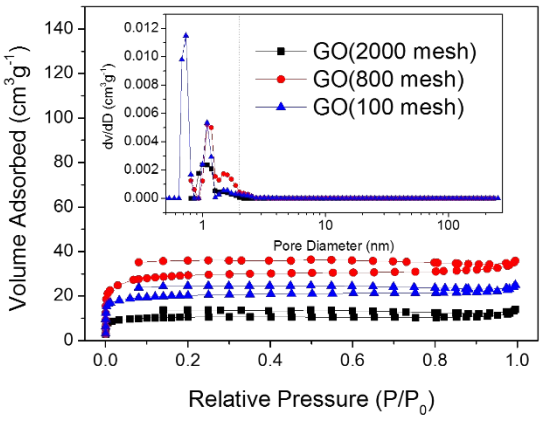

Fig. 5. Nitrogen adsorption-desorption isotherms and pore size distribution curve (inset) of GO (2000 mesh), GO (800 mesh), and GO (100 mesh).

Electrochemical analysis

The cyclic voltammogram analysis is a universal method to evaluate the capacitive behavior. As is known, the GO has low conductivity. And the square resistances of GO samples are about 120 MOhm/sq measured by four-point probe meter. Therefore a small quantity of carbon black was added to electrode and nickel foam was used as current collecter. The CV curves of nickel foam and the three GO electrodes at 50 m V s^{-1} are shown in Fig. 6(a). Obviously, the current collector, nickel foam, has a negligible capacitance. The integrated areas for the GO electrodes intuitively grow with the increase of raw graphite size, which is an indication of superior capacity and rapid diffusion of electrolyte ions from the solution into the pores of the electrode from larger raw materials. As shown in Fig. 6(b)-(d), the CV curves of GO (2000 mesh), GO (800 mesh), GO (100 mesh) measured at low scan rates, exhibit an almost rectangular shape, while the CV curves become a little distorted at a high scan rate. Xu et al. investigated the rate capability of GO electrodes and demonstrated that the containing-oxygen functional groups could participate in quick pseudo-faradaic charge-discharge reactions. That means GO electrodes have a quick charge propagation capability of both double layer capacitance and pseudo-capacitance[15].

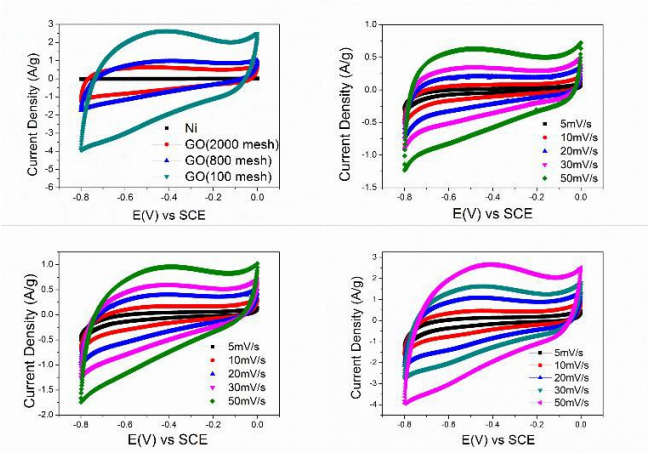

Fig. 6 (a) Cyclic voltammograms of different electrode materials at 50 m Vs^{-1}, cyclic voltammograms at different voltage scanning rates of (b) GO (2000 mesh), (c) GO (800 mesh), (d) GO (100 mesh).

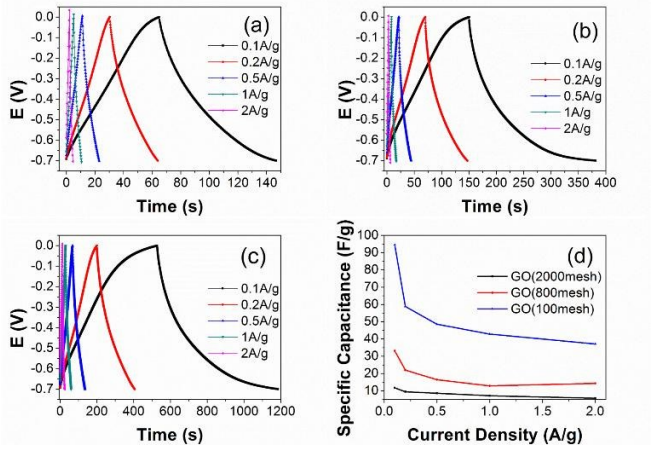

Fig. 7. Galvanic cycle curves for GO electrodes on nickel foam (a) GO (2000 mesh), (b) GO (800 mesh), (c) GO (100 mesh), (d) Specific capacitance as a function of current density in 6M KOH for all samples.

To obtain the more accurate specific capacitance of the GO electrodes for supercapacitors, galvanic cycle test was further performed, according to Eq. (2).

$$C = (I \cdot \Delta t)/(m \cdot \Delta U) \quad (2)$$

where, I is the applied current (A), Δt is the discharge time (s), ΔU is potential range, m is the mass of active materials, Fig. 7(a)-(c) exhibit the charge-discharge cycle curves of GO electrodes at different current densities. The GO (100 mesh), GO (800 mesh) and GO (2000 mesh) electrodes deliver an initial specific capacitance of 94.4, 33.1 and 11.7 F g^{-1}, respectively, at the current density of 0.1 A g^{-1}. Fig. 7(d) shows the specific capacitance as a function of current density in 6M KOH for all samples. A decrease in specific capacitance was observed at high current densities owing to the slow diffusion of the electrolyte ions into the porous of GO electrode during the fast charge/discharge process[31, 32].

The typical Nyquist plots of the GO electrodes are shown in Fig. 8. The plots consist of a small semicircle at the high frequency region, which reflects the charge transfer process, and the inclined line in the low frequency range, representing the Warburg impedance, which shows the quick adsorption of ions onto the electrode surface and fast diffusion of ions. The observed equivalent series resistance (ESR) of GO (2000 mesh), GO (800 mesh), GO (100 mesh) are similar and the charge transfer resistances of them decrease with the increase of raw graphite sizes. What's more, GO (100 mesh) has the fast diffusion of ions while GO (800 mesh) has the worst of that, which may ascribe to different porous structure. Base on above experimental results, the GO (800 mesh) possesses the largest specific surface area yet the corresponding electrode does not own the highest specific capacitance, among the GOs prepared from three different size of raw graphite. The reason is that the electrode with GO (800 mesh) has larger charge transfer resistance and the lowest diffusion of ions. Hence, it could be concluded that the capacitive properties GO-based electrodes displaying on supercapacitors are highly dependent on the pore structure, specific surface area and electrical conductance properties.

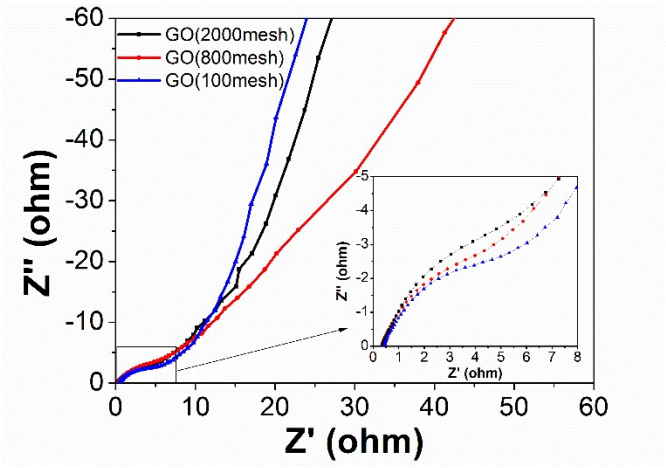

Fig. 8. The Nyquist plots of three GO electrodes (the inset shows the enlarged EIS at high frequency region).

The cycling lifetime is another important requirement to judge the electrochemical performances of electrodes. As shown in Fig. 9, there is almost no attenuation for the specific capacitance of all three GO electrodes after 1500 cycles, indicating all these GOs have outstanding cycling stability. The XPS spectra of C1s in GO (100 mesh) after 1500 cycles shows that some oxygen-containing functional groups were removed. (Supporting Information Fig. S2) And the molar ratios of C/O of it increased to 2.7 from 2.2, which means at least 82% content of oxygen-containing functional groups are stable to maintain high capacitance.

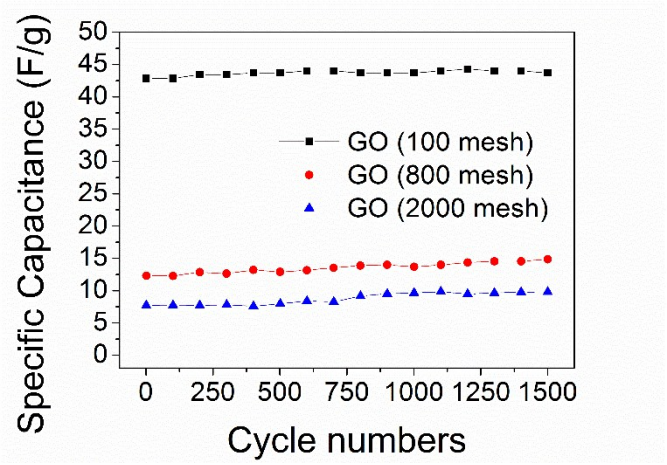

Fig. 9. Specific capacitance of GO electrodes for a 1500-cycles charge-discharge test at current densities of 1A g-1.

Conclusions

To sum up, the comparison of electrochemical performances of GO electrodes with three different raw graphite size were systematically investigated. The specific capacitance of electrodes was 94.4, 33.1 and 11.7 F g^{-1} for GO (100 mesh), GO (800 mesh) and GO (2000 mesh), respectively, at the current density of 0.1 A g^{-1}. The capacitance of the GO electrodes is enhanced with the increasing size of the raw graphite. That is because the specific surface area and charge transfer resistance simultaneously have significant influence on performances of the GO electrodes. At the same time, the three GO electrodes possess preeminent cycling stability.

As for the problem appeared in the synthesis of GO, the decrease of specific surface area is the contribution of hydrogen bonding interactions caused by intercalated water molecules. Further, small particles are more likely to agglomerate or even restacking because of strong interactions between GO layers. Thus, more attention should be paid on the problem in terms of synthesizing graphene oxide-based electrode materials for supercapacitors or other energy storage devices.

Acknowledgements

The authors acknowledge the financial support of this work by the National Natural Science Foundation of China (51302219, 51472204 and 51402236), the Natural Science Foundation of Shannxi Province (2015JM2045), the Research Fund of the State Key Laboratory of Solidification Processing (NWPU), China (Grant No.06-QP-2014), and the Fundamental Research Funds for the Central Universities (3102014JCQ01019 and 3102015BJ(II)MYZ02).

Notes and references

1 C. Liu, Z. Yu, D. Neff, A. Zhamu and B. Z. Jang, Nano Letters, 2010, 10, 4863-4868.
2 Y. Wang, Z. Shi, Y. Huang, Y. Ma, C. Wang, M. Chen and Y. Chen, J. Phys. Chem. C, 2009, 113, 13103-13107.
3 Y. A. Kim, T. Hayashi, J. H. Kim and M. Endo, J. Energ. Chem., 2013, 22, 183-194.
4 M. D. Stoller, S. Park, Y. Zhu, J. An and R. S. Ruoff, Nano Letters, 2008, 8, 3498-3502.
5 Q. Zhang, K. Scrafford, M. Li, Z. Cao, Z. Xia, P. M. Ajayan and B. Wei, Nano Letters, 2014, 14, 1938-1943.
6 Y. Huang, J. Liang and Y. Chen, Small, 2012, 8, 1805-1834.
7 E. B. Secor, P. L. Prabhumirashi, K. Puntambekar, M. L. Geier and M. C. Hersam, J. Phys. Chem. Lett., 2013, 4, 1347-1351.
8 T. Yumura and A. Yamasaki, Phys. Chem. Chem. Phys., 2014, 16, 9656-9666.
9 X. Wang and G. Shi, Energy Environ. Sci., 2015, 8, 790-823.
10 B. Lobato, R. Wendelbo, V. Barranco and T. A. Centeno, Electrochim. Acta, 2014, 149, 245-251.
11 C. Soldano, A. Mahmood and E. Dujardin, Carbon, 2010, 48, 2127-2150.
12 C. H. Lui, L. Liu, K. F. Mak, G. W. Flynn and T. F. Heinz, Nature, 2009, 462, 339-341.
13 P. W. Sutter, J. I. Flege and E. A. Sutter, Nat. Mater., 2008, 7, 406-411.
14 F. Su, C. K. Poh, J. S. Chen, G. Xu, D. Wang, Q. Li, J. Lin and X. W. Lou, Energy Environ. Sci., 2011, 4, 717-724.
15 B. Xu, S. Yue, Z. Sui, X. Zhang, S. Hou, G. Cao and Y. Yang, Energy Environ. Sci., 2011, 4, 2826.
16 W. S. Hummers, Jr. and R. E. Offema, J. Am. Chem. Soc., 1958, 1339-1339.
17 X. Zhang, K. Li, H. Li and J. Lu, J. Colloid Interface Sci., 2013, 409, 1-7.
18 A. C. Ferrari, Solid State Commun., 2007, 143, 47-57.
19 L. M. Malard, M. A. Pimenta, G. Dresselhaus and M. S. Dresselhaus, Phys. Rep., 2009, 473, 51-87.
20 Z. Ni, Y. Wang, T. Yu and Z. Shen, Nano Res., 2010, 1, 273-291.
21 Z. H. Ni, T. Yu, Y. H. Lu, Y. Y. Wang, Y. P. Feng and Z. X. Shen, ACS nano, 2008, 2301-2305.
22 S. Park and R. S. Ruoff, Nat. Nanotechnol., 2009, 4, 217-224.
23 D. R. Dreyer, S. Park, C. W. Bielawski and R. S. Ruoff, Chem. Soc. Rev., 2009, 39, 228–240.
24 Y. Yoon, K. Lee, C. Baik, H. Yoo, M. Min, Y. Park, S. M. Lee and H. Lee, Adv. Mater., 2013, 25, 4437-4444.
25 M. Acik, C. Mattevi, C. Gong, G. Lee, K. Cho, M. Chhowalla and Y. J. Chabal, ACS Nano, 2010, 4, 5861–5868.
26 J. H. Lee, N. Park, B. G. Kim, D. S. Jung, K. Im, J. Hur and J. W. Choi, ACS Nano, 2013.
27 A. Dimiev and J. M. Tour, ACS Nano, 2014, 8, 3060–3068.
28 M. Kruk and M. Jaroniec, Chem. Mater., 2000, 12, 1961-1968.
29 M. Kruk and M. Jaroniec, Chem. Mater., 2001, 13, 3169-3183.
30 R. Ryoo, I.-S. Park, S. Jun, C. W. Lee, M. Kruk and M. Jaroniec, J. Am. Chem. Soc., 2001, 123, 1650-1657.
31 Y. Li, M. Zhou, X. Cui, Y. Yang, P. Xiao, L. Cao and Y. Zhang, Electrochim. Acta, 2015, 161, 137-143.
32 R. N. Reddy and R. G. Reddy, J. Power Sources, 2006, 156, 700-704.

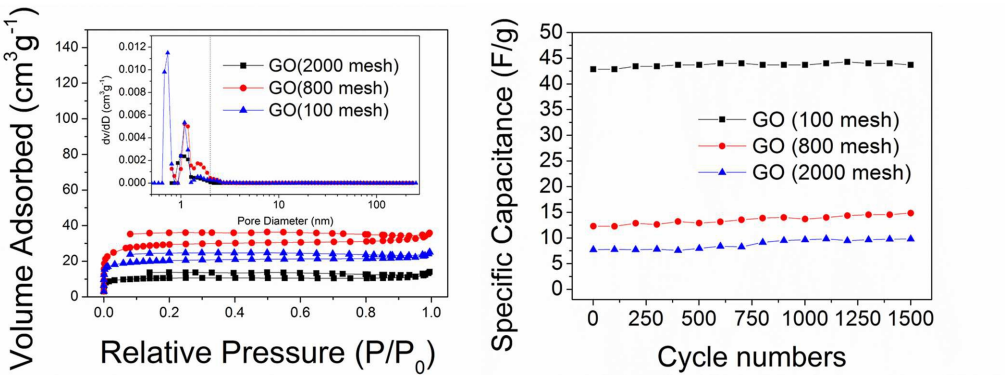

The importance of raw graphite size to the capacitive properties of graphene oxides was discussed.